Journal of Solid Mechanics Vol. 1, No. 4 (2009) pp. 271-288

Temperature Effects on Nonlinear Vibration of FGM Plates Coupled with Piezoelectric Actuators

F. Ebrahimi*, A. Rastgoo

Faculty of Mechanical Engineering, College of Engineering, University of Tehran, Tehran, Iran

Received 23 August 2009; accepted 11 December 2009

ABSTRACT

An analytical solution for a sandwich circular FGM plate coupled with piezoelectric layers under one-dimension heat conduction is presented in this paper. A nonlinear static problem is solved first to determine the initial stress state and pre-vibration deformations. By adding an incremental dynamic state to the pre-vibration state, the differential equations are derived. The role of thermal environment and control effects on nonlinear static deflections and natural frequencies imposed by the piezoelectric actuators using high input voltages are investigated. The good agreement between the results of this paper and those of the finite element (FE) analyses validated the presented approach. The emphasis is placed on investigating the effect of varying the applied actuator voltage and thermal environment as well as gradient index of FG plate on the dynamics and control characteristics of the structure.

Keywords: FGM plate; Nonlinear vibration; Piezoelectric actuators

1 INTRODUCTION

THE concept of developing smart structures has been extensively used for active control of flexible structures during the past decade. In this regard, the use of axisymmetric piezoelectric actuators in the form of a disc or ring to produce motion in a circular or annular substrate plate is common in a wide range of applications including micro-pumps and micro-valves [1] and implantable medical devices [2]. Functionally graded materials (FGMs) are a new generation of composite materials wherein the material properties vary continuously to yield a predetermined composition profile. These materials have been introduced to benefit from the ideal performance of its constituents, e.g., high heat/corrosion resistance of ceramics on one side, and large mechanical strength and toughness of metals on the other side. FGMs have no interfaces and are hence advantageous over conventional laminated composites. FGMs also permit tailoring of material composition to optimize a desired characteristic such as minimize the maximum deflection for a given load and boundary conditions, or maximize the first frequency of free vibration, or minimize the maximum principal tensile stress. FGMs are now developed for the general use as structural components and specially to operate in environments with extremely high temperatures. Low thermal conductivity, low coefficient of thermal expansion and core ductility have enabled the FGM materials to withstand higher temperature gradients for a given heat flux. Structures made of FGMs are often susceptible to failure from large deflections, or excessive stresses that are induced by large temperature gradients and/or mechanical loads. It is therefore of prime importance to account for the geometrically nonlinear deformation as well as the thermal environment effect to ensure more accurate and reliable structural analysis and design.

Also in recent years, with the increasing use of smart material in vibration control of plate structures, the mechanical response of FGM plates with surface-bonded piezoelectric layers has attracted some researchers' attention. Since this area is relatively new, published literature on the free and forced vibration of FGM plates is

* Corresponding author.
E-mail address: febrahimy@ut.ac.ir (F. Ebrahimi).

limited and most of them are focused on the cases of the linear problem. Among those, a 3-D solution for rectangular FG plates coupled with a piezoelectric actuator layer was proposed by Reddy and Cheng [3] using transfer matrix and asymptotic expansion techniques. Wang and Noda [4] analyzed a smart FG composite structure composed of a layer of metal, a layer of piezoelectric and an FG layer in between, while Huang and Shen [5] investigated the dynamics of an FG plate coupled with two monolithic piezoelectric layers at its top and bottom surfaces undergoing nonlinear vibrations in thermal environments. All the aforementioned studies focused on the rectangular-shaped plate structures.

To the authors' best knowledge, no researches dealing with the nonlinear vibration characteristics of the circular FGM plate integrated with piezoelectric layers have been reported in literature except the author's recent works in free axisymmetric linear vibration analysis of piezoelectric coupled circular and annular FGM plates [6, 7] and investigating the applied control voltage effect on piezoelectrically actuated FG circular plate [8] in which the thermal environment effects are not taken into account. Consequently, a non-linear dynamics and vibration analysis are conducted on pre-stressed piezo-actuated FG circular plates in thermal environment. Nonlinear governing equations of motion are derived based on Kirchhoff's-Love hypothesis with von-Karman type geometrical large nonlinear deformations. An exact series expansion method combined with perturbation approach is used to model the non-linear thermo-electro-mechanical vibration behavior of the structure. Numerical results for FG plates with various mixture of ceramic and metal are presented in dimensionless forms. A parametric study is also undertaken to highlight the effects of the thermal environment, applied actuator voltage and material composition of FG core plate on the nonlinear vibration characteristics of the composite structure.

2 MATERIAL PROPERTIES

Nowadays not only FGM can easily be produced but one can control even the variation of the FG constituents in a specific way. For example in an FG material made of ceramic and metal mixture, we have;

$$V_m + V_c = 1 \tag{1}$$

in which V_c and V_m are the volume fraction of the ceramic and metallic part, respectively. Based on the power law distribution [9], the variation of V_c vs. thickness coordinates (z) with its origin placed at the middle of thickness can be expressed as;

$$V_c = (z/2h_f + 1/2)^n, \qquad n \geq 0 \tag{2}$$

in which h_f is the FG core plate thickness and n is the FGM volume fraction index. We assume that the inhomogeneous material properties, such as the modulus of elasticity E, density ρ, thermal expansion coefficient α and the thermal conductivity κ change within the thickness direction z based on Voigt's rule over the whole range of the volume fraction while the Poisson's ratio υ is assumed to be constant in the thickness direction [8] as;

$$\begin{aligned} E(z) &= (E_c - E_m)V_c(z) + E_m \\ \rho(z) &= (\rho_c - \rho_m)V_c(z) + \rho_m \\ \kappa(z) &= (\kappa_c - \kappa_m)V_c(z) + \kappa_m \\ \alpha(z) &= (\alpha_c - \alpha_m)V_c(z) + \alpha_m \\ \nu(z) &= \nu \end{aligned} \tag{3}$$

where subscripts m and c refer to the metal and ceramic constituents, respectively. After substituting V_c from Eq. (2) into Eqs. (3), material properties of the FGM plate are determined in the power law form which are the same as those proposed by Reddy and Praveen [9] i.e.;

$$\begin{aligned} E_f(z) &= (E_c - E_m)(z/2h_f + 1/2)^n + E_m \\ \rho_f(z) &= (\rho_c - \rho_m)(z/2h_f + 1/2)^n + \rho_m \\ \kappa_f(z) &= (\kappa_c - \kappa_m)(z/2h_f + 1/2)^n + \kappa_m \end{aligned} \tag{4}$$

$$\alpha_f(z) = (\alpha_c - \alpha_m)(z/2h_f + 1/2)^n + \alpha_m$$

3 THERMAL ENVIRONMENT

Assuming piezo-laminated FGM plate is subjected to the thermal environment and the temperature variation occurs in the thickness direction and 1D temperature field is assumed to be constant in the r-θ plane of the plate. In such a case, the temperature distribution along the thickness can be obtained by solving a steady-state heat transfer equation [5]

$$-\frac{\mathrm{d}}{\mathrm{d}z}\left[\kappa(z)\frac{\mathrm{d}T}{\mathrm{d}z}\right] = 0 \tag{5}$$

in which

$$\kappa(z) = \begin{cases} \kappa_p & (h_f/2 < z < h_p + h_f/2) \\ \kappa_f(z) & (-h_f/2 < z < h_f/2) \\ \kappa_p & (-h_p - h_f/2 < z < -h_f/2) \end{cases} \tag{6}$$

$$T(z) = \begin{cases} T_p(z) & (h_f/2 \le z \le h_p + h_f/2) \\ T_f(z) & (-h_f/2 \le z \le h_f/2) \\ \tilde{T}_p(z) & (-h_p - h_f/2 \le z \le -h_f/2) \end{cases} \tag{7}$$

where κ_p and κ_f are the thermal conductivity of piezoelectric layers and FG plate respectively. Eq. (5) is solved by imposing the boundary conditions as

$$T_p\big|_{z=h_p+h_f/2} = T_U \qquad \tilde{T}_p\big|_{z=-h_p-h_f/2} = T_L \tag{8}$$

and the continuity conditions

$$\begin{aligned} &T_p\big|_{z=h_f/2} = T_f\big|_{z=h_f/2} = T_1 \quad T_f\big|_{z=-h_f/2} = \tilde{T}_p\big|_{z=-h_f/2} = T_2 \\ &\kappa_p \left.\frac{\mathrm{d}T_p(z)}{\mathrm{d}z}\right|_{z=h_f/2} = \kappa_c \left.\frac{\mathrm{d}T_f(z)}{\mathrm{d}z}\right|_{z=h_f/2} \\ &\kappa_p \left.\frac{\mathrm{d}\tilde{T}_p(z)}{\mathrm{d}z}\right|_{z=-h_f/2} = \kappa_m \left.\frac{\mathrm{d}T_f(z)}{\mathrm{d}z}\right|_{z=-h_f/2} \end{aligned} \tag{9}$$

The solution of Eq. (5) with the aforementioned conditions can be expressed as polynomial series

$$T_p(z) = T_1 + \frac{T_U - T_1}{h_p}(z - h_f/2) \tag{10}$$

$$\tilde{T}_p(z) = T_L + \frac{T_2 - T_L}{h_p}(z + h_f/2 + h_p) \tag{11}$$

and

$$T_f(z) = A_0 + A_1\left(\frac{z}{h_f}+\frac{1}{2}\right) + A_2\left(\frac{z}{h_f}+\frac{1}{2}\right)^{N+1} + A_3\left(\frac{z}{h_f}+\frac{1}{2}\right)^{2N+1} + A_4\left(\frac{z}{h_f}+\frac{1}{2}\right)^{3N+1} + A_5\left(\frac{z}{h_f}+\frac{1}{2}\right)^{4N+1} + A_6\left(\frac{z}{h_f}+\frac{1}{2}\right)^{5N+1} + O(z)^{6N+1} \tag{12}$$

where constants T_1, T_2 and A_j can be found in Appendix A.

4 THEORY

It is assumed that an FGM circular plate is sandwiched between two thin piezoelectric layers which are sensitive in both circumferential and radial directions and the structure is in thermal environment, also the piezoelectric layers are much thinner than the FGM plate, i.e., $h_p << h_f$ .An initial large deformation exceeding the linear range is imposed on the circular plate and the von-Karman type nonlinear deformation is adopted in the analysis. The von-Karman type nonlinearity assumes that the transverse nonlinear deflection w is much more prominent than the other two in-plane deflections. Based on Kirchhoff's-Love assumptions, the strain components at distance z from the middle plane are given by

$$\varepsilon_{rr} = \bar{\varepsilon}_{rr} + zk_{rr}, \quad \varepsilon_{\theta\theta} = \bar{\varepsilon}_{\theta\theta} + zk_{\theta\theta}, \quad \varepsilon_{r\theta} = \bar{\varepsilon}_{r\theta} + zk_{r\theta} \tag{13}$$

Here $\bar{\varepsilon}_{rr}$, $\bar{\varepsilon}_{\theta\theta}$, $\bar{\varepsilon}_{r\theta}$ are the engineering strain components in the median surface, and k_{rr} , $k_{\theta\theta}$, $k_{r\theta}$ are the curvatures which can be expressed in terms of the displacement components. The relations between the middle plane strains and the displacement components according to the von-Karman type nonlinear deformation and Sander's assumptions [10] are defined as:

$$\begin{aligned}
&\bar{\varepsilon}_{rr} = \frac{\partial u_r}{\partial r} + \frac{1}{2}\left(\frac{\partial w}{\partial r}\right)^2, \quad \kappa_{r\theta} = -\frac{1}{r}\left(\frac{\partial^2 w}{\partial r \partial \theta}\right) + \frac{1}{2r^2}\frac{\partial w}{\partial \theta} \\
&\bar{\varepsilon}_{\theta\theta} = \frac{1}{r}\frac{\partial u_\theta}{\partial \theta} + \frac{u_r}{r} + \frac{1}{2}\left(\frac{1}{r}\frac{\partial w}{\partial \theta}\right)^2, \quad \kappa_{\theta\theta} = -\frac{1}{r}\frac{\partial w}{\partial r} - \frac{1}{r^2}\frac{\partial^2 w}{\partial \theta^2} \\
&\bar{\varepsilon}_{r\theta} = \frac{1}{r}\frac{\partial u_r}{\partial \theta} + \frac{\partial u_\theta}{\partial r} - \frac{u_\theta}{r} + \left(\frac{1}{r}\frac{\partial w}{\partial r}\right)\frac{\partial w}{\partial \theta}, \ \kappa_{rr} = -\frac{\partial^2 w}{\partial r^2}
\end{aligned} \tag{14}$$

where u_r , u_θ ,w represent the corresponding components of the displacement of a point on the middle plate surface. Substituting Eqs. (14) into Eqs. (13), the following expressions for the strain components are obtained

$$\begin{aligned}
&\varepsilon_{rr} = \frac{\partial u_r}{\partial r} + \frac{1}{2}\left(\frac{\partial w}{\partial r}\right)^2 - z\frac{\partial^2 w}{\partial r^2} \\
&\varepsilon_{\theta\theta} = \frac{1}{r}\frac{\partial u_\theta}{\partial \theta} + \frac{u_r}{r} + \frac{1}{2}\left(\frac{1}{r}\frac{\partial w}{\partial \theta}\right)^2 - z\left(\frac{1}{r}\frac{\partial w}{\partial r} + \frac{1}{r^2}\frac{\partial^2 w}{\partial \theta^2}\right) \\
&\varepsilon_{r\theta} = \frac{1}{r}\frac{\partial u_r}{\partial \theta} + \frac{\partial u_\theta}{\partial r} - \frac{u_\theta}{r} + \left(\frac{1}{r}\frac{\partial w}{\partial r}\right)\frac{\partial w}{\partial \theta} + 2z\left(-\frac{1}{r}\left(\frac{\partial^2 w}{\partial r \partial \theta}\right) + \frac{1}{2r^2}\frac{\partial w}{\partial \theta}\right)
\end{aligned} \tag{15}$$

For a circular plate with axisymmetric oscillations, the strain expressions are simplified to

$$\varepsilon_{rr} = \frac{\partial u_r}{\partial r} + \frac{1}{2}\left(\frac{\partial w}{\partial r}\right)^2 - z\frac{\partial^2 w}{\partial r^2}$$
$$\varepsilon_{\theta\theta} = \frac{u_r}{r} - \frac{z}{r}\frac{\partial w}{\partial r} \tag{16}$$
$$\varepsilon_z = \gamma_{r\theta} = \gamma_{\theta z} = \gamma_{zr} = 0$$

The stress components in the FG core plate in terms of strains based on the generalized Hooke's Law using the plate theory approximation of $\sigma_z \approx 0$ in the constitutive equations are defined as [11];

$$\sigma_r^f = \frac{E(z)}{1-\nu^2}(\varepsilon_r + \nu\varepsilon_\theta) - \frac{E(z)\alpha(z)}{1-\nu}\Delta T \tag{17}$$

$$\sigma_\theta^f = \frac{E(z)}{1-\nu^2}(\varepsilon_\theta + \nu\varepsilon_r) - \frac{E(z)\alpha(z)}{1-\nu}\Delta T \tag{18}$$

where $E(z)$, $\nu(z)$ and $\alpha(z)$ are Young's modulus, Poisson's ratio and coefficient of thermal expansion of the FGM material respectively as expressed in Eq.(4) ; where $\Delta T = T(z) - T_0$ is temperature rise from the stress-free reference temperature (T_0) which is assumed to exist at a temperature of $T_0 = 0$ and $T(z)$ is presented in Eqs. (10)-(12). The moments and membrane forces include both mechanical and electric components as

$$N_r = N_r^m - N_r^e - N_r^t, \quad N_\theta = N_\theta^m - N_\theta^e - N_\theta^t \ , \tag{19}$$

$$M_r = M_r^m - M_r^e - M_r^t, \quad M_\theta = M_\theta^m - M_\theta^e - M_\theta^t \tag{20}$$

where the superscripts *m*, *e*, and *t*, respectively, denote the mechanical, electric, and temperature components. Mechanical forces and moments of the thin circular plate made of functionally graded material can be expressed as

$$(N_r^m, N_\theta^m) = \int_{-h_f/2}^{h_f/2} (\sigma_{rr}, \sigma_{\theta\theta})\, \mathrm{d}z \tag{21}$$

$$(M_r^m, M_\theta^m) = \int_{-h_f/2}^{h_f/2} (\sigma_{rr}, \sigma_{\theta\theta})\, z\, \mathrm{d}z \tag{22}$$

$$(N_{r\theta}^m, M_{r\theta}^m) = \int_{-h_f/2}^{h_f/2} (1, z)\sigma_{r\theta}\, \mathrm{d}z \tag{23}$$

Substituting Eqs. (13), (17), and (18) into Eqs. (22) and (23) gives the following constitutive relations for mechanical forces and moments of FG plate :

$$N_r^m = D_1(\bar{\varepsilon}_{rr} + \nu\bar{\varepsilon}_{\theta\theta}), \quad N_\theta^m = D_1(\bar{\varepsilon}_{\theta\theta} + \nu\bar{\varepsilon}_{rr}) \tag{24}$$

$$M_r^m = D_2(\kappa_{rr} + \nu\kappa_{\theta\theta}), \quad M_\theta^m = D_2(\kappa_{\theta\theta} + \nu\kappa_{rr}) \tag{25}$$

$$N_r^t = N_\theta^t = \int_{-h_t/2}^{h_t/2} \frac{\alpha(z)E(z)}{1-\nu}\Delta T(z)\, \mathrm{d}z \tag{26}$$

$$M_r^t = M_\theta^t = \int_{-h_t/2}^{h_t/2} \frac{\alpha(z)E(z)}{1-\nu}\Delta T(z)\, z\, \mathrm{d}z \tag{27}$$

in which the coefficients of D_1 and D_2 in the above equations are related to the plate stiffness and are given by

$$D_1 = \int_{-h_f/2}^{h_f/2} \frac{E_f(z)}{1-\nu_f^2}\,\mathrm{d}z \quad , \; D_2 = \int_{-h_f/2}^{h_f/2} z^2 \frac{E_f(z)}{1-\nu_f^2}\,\mathrm{d}z \tag{28}$$

It is assumed that the piezoelectric layers are sensitive in both radial and circumferential directions and the piezoelectric permeability constants e_{31}=e_{32}. Hence, the electric membrane forces and bending moments vary linearly as

$$N_r^e = N_\theta^e = -e_{31}(V_z^t + V_z^b)/2, \tag{29}$$

$$M_r^e = M_\theta^e = -e_{31}(h_f + h_p)(V_z^t - V_z^b)/2 \tag{30}$$

in which V_z^t and V_z^b are the control voltages applied to the top and bottom piezoelectric layers respectively. Axisymmetric free oscillation equations of the piezoelectric coupled circular FG plate in thermal environment can be derived from the generic piezoelectric shell equations using four system parameters: two Lame parameters, i.e., $A_1 = 1$, $A_2 = r$, where r is the radial distance measured from the center and two radii, i.e., $R_1 = \infty$, $R_2 = \infty$ [12,13] as

$$\frac{\partial(rN_r)}{\partial r} - N_\theta = 0 \tag{31}$$

$$\frac{1}{r}\frac{\partial(rQ_{rz})}{\partial r} + N_r\frac{\partial^2 w}{\partial r^2} + N_{\theta\theta}\left(\frac{1}{r}\frac{\partial w}{\partial \theta}\right) - I_1\frac{\partial^2 w}{\partial t^2} = 0 \tag{32}$$

in which $I_1 = \left(\int_{-h_f/2}^{h_f/2} \rho_f(z)\,\mathrm{d}z\right)$ and the transverse shear component Q_{rz} is related to moments as

$$Q_{rz} = \frac{1}{r}\left[\frac{\partial(rM_r)}{\partial r} - M_\theta\right] \tag{33}$$

Substituting all force/moment components and strain-displacement equations into the radial and transverse equations (31), (32) yields

$$r\frac{\partial}{\partial r}\left[\frac{1}{r}\frac{\partial}{\partial r}\left(r^2 N_r^m\right)\right] = -\frac{Y}{2}\left(\frac{\partial w}{\partial r}\right)^2 + \frac{\partial}{\partial r}\left[r^2\frac{\partial}{\partial r}\left(N_r^e + N_r^t\right)\right] + \nu\, r\frac{\partial}{\partial r}\left(N_r^e + N_r^t\right) \tag{34}$$

$$\frac{D_2}{r}\frac{\partial}{\partial r}\left(r\frac{\partial}{\partial r}\left[\frac{1}{r}\frac{\partial}{\partial r}\left(r\frac{\partial}{\partial r}w(r,t)\right)\right]\right) = -I_1\frac{\partial^2 w}{\partial t^2} + \frac{1}{r}\frac{\partial}{\partial r}\left[r\frac{\partial w}{\partial r}\left(N_r^m - N_r^e - N_r^t\right)\right] - \frac{1}{r}\frac{\partial}{\partial r}\left[r\frac{\partial}{\partial r}\left(M_r^e + M_r^t\right)\right] \tag{35}$$

in which $Y = \int_{-h_f/2}^{h_f/2} E_f(z)\,\mathrm{d}z$ and boundary conditions at the center of the plate with axisymmetric oscillations are defined as

(1) Plate center (r=0):

Slope: $\frac{\partial w}{\partial r} = 0$ (36a)

Radial force: N_{rr}^m : finite (36b)

Boundary conditions for the simply supported (immovable) circumference are defined as:

(2) Plate circumference (r=a):

$w = 0$ (37a)

$$\frac{\partial}{\partial r}(rN_r^m) - \nu N_r^m = r\frac{\partial}{\partial r}(N_r^e + N_r^t) \tag{37b}$$

$$-D_2\left(\frac{\partial^2 w}{\partial r^2} + \frac{\nu}{r}\frac{\partial w}{\partial r}\right) = (M_r^e + M_r^t) \tag{37c}$$

It is further assumed that the control potentials on top and bottom piezoelectric actuators are of equal magnitudes and opposite signs, i.e $V_z^t = -V_z^b = \hat{V}$ and the plate is subjected to a uniform temperature excitation of $T(z)$. Accordingly, the electric and temperature induced forces and moments can be defined as:

$$N_r^e = N_\theta^e = 0 \tag{38a}$$

$$M_r^e = M_\theta^e = M^e = -e_{31}\left(h_f + h_p\right)\hat{V} \tag{38b}$$

$$N_\theta^t = N_r^t = N^t \tag{39a}$$

$$M_\theta^t = M_r^t = M^t \tag{39b}$$

Using these force and moment expressions, one can further simplify the open-loop plate equations and boundary conditions

$$r\frac{\partial}{\partial r}\left[\frac{1}{r}\frac{\partial}{\partial r}\left(r^2 N_r^m\right)\right] = -\frac{Y}{2}\left(\frac{\partial w}{\partial r}\right)^2 \tag{40}$$

$$\frac{D_2}{r}\frac{\partial}{\partial r}\left(r\frac{\partial}{\partial r}\left[\frac{1}{r}\frac{\partial}{\partial r}\left(r\frac{\partial}{\partial r}w(r,t)\right)\right]\right) = -I_1\frac{\partial^2 w}{\partial t^2} + \frac{1}{r}\frac{\partial}{\partial r}\left[r\frac{\partial w}{\partial r}(N_r^m - N^t)\right] \tag{41}$$

Boundary conditions become

(1) Plate center (r=0):

Slope: $\left.\frac{\partial w}{\partial r}\right|_{r=0}$ (42a)

Radial force: $N_r^m\big|_{r=0}$: finite (42b)

(2) Plate circumference (r=a):

$$w\big|_{r=a} = 0 \tag{43a}$$

$$\left[\frac{\partial}{\partial r}(rN_r^m) - \nu N_r^m\right]_{r=a} = 0 \tag{43b}$$

$$\left[-D_2\left(\frac{\partial^2 w}{\partial r^2} + \frac{\nu}{r}\frac{\partial w}{\partial r}\right)\right]_{r=a} = (M^e + M^t) \tag{43c}$$

Solutions of the transverse displacement w and radial force N_r^m of the above open-loop plate equations and boundary conditions can be expressed as a summation of a static component and a dynamic component as

$$w(r,t) = w_s(r) + w_d(r,t)\,, \tag{44a}$$

$$N_r^m(r,t) = N_{r_s}^m(r,t) + N_{r_d}^m(r,t) \tag{44b}$$

where $w_s(r)$ and $N_{r_s}^m(r,t)$ are the static solutions; $w_d(r,t)$ and $N_{r_d}^m(r,t)$ are the dynamic solutions; and the subscripts *s* and *d*, respectively, denote the static and dynamic solutions. Accordingly, the solution procedures can be divided into two parts. The first part deals with the nonlinear static solutions and the second part deals with the dynamic solutions. In addition, normalized dimensionless quantities are adopted in the static and dynamic analyses. These dimensionless quantities are defined by known geometrical and material parameters [14]:

- radial distance: $y = (r/a)^2$
- transverse deflection: $\bar{w}_s = \sqrt{3(1-\nu^2)}w_s / h_f$
- slope: $X_s(y) = y\dfrac{d\bar{w}_s}{dy}$
- static force: $Y_s^m(y) = (a^2 N_{r_s}^m / 4D_2)y$
- temperature load: $T^* = (a^2 N^t / 4D_2)$
- radial distance: $x = (r/a)$
- dynamic deflection: $\bar{w}_d = \sqrt{3(1-\nu^2)}w_d / h_f$
- dynamic force: $Y_d^m(y) = (a^2 N_{r_d}^m / D_2)$
- voltage: $V = \left[3(1-\nu^2)\right]^{1/2} e_{31}(h_f + h_p)\hat{V} / (2D_2 h_f)$

Substituting these normalized dimensionless quantities into the open-loop plate equations and boundary conditions of axisymmetric plate oscillations and separating the static parts from the dynamic parts gives the static equations and dynamic equations with their associated boundary conditions:

(A) Static equations and boundary conditions

$$y^2\frac{d^2X_s}{dy^2} = X_s Y_s^m - T^* y X_s \tag{45}$$

$$y^2\frac{d^2Y_s^m}{dy^2} = -\frac{1}{2}\left(X_s\right)^2, \qquad 0 < y < 1 \tag{46}$$

Boundary conditions at center $y = 0$:

$$X_s\big|_{y=0} = 0 \tag{47a}$$

$$Y_s^m\Big|_{y=0} = 0 \tag{47b}$$

Boundary conditions on circumference $y = 1$:

$$\left[\left(1+\nu\right)Y_s^m - 2\frac{\mathrm{d}Y_s^m}{\mathrm{d}y}\right]_{y=1} = 0, \tag{48a}$$

$$\left[\left(1-\nu\right)\frac{X_s}{y} - 2\frac{\mathrm{d}X_s}{\mathrm{d}y}\right]_{y=1} = V\big|_{y=1} \tag{48b}$$

(B) Dynamic equations and boundary conditions

$$x\frac{\partial}{\partial x}\left(\frac{1}{x}\frac{\partial}{\partial x}\left[x^2 Y_d^m\right]\right) = -2\left[\frac{\mathrm{d}\bar{w}_s}{\mathrm{d}x}\frac{\partial\bar{w}_d}{\partial x} - \frac{1}{2}\left(\frac{\partial\bar{w}_d}{\partial x}\right)^2\right] \tag{49}$$

$$\frac{1}{x}\frac{\partial}{\partial x}\left\{x\frac{\partial}{\partial x}\left[\frac{1}{x}\frac{\partial}{\partial x}\left(x\frac{\partial}{\partial x}(\bar{w}_d)\right)\right]\right\}= \tag{50}$$

$$-\frac{I_1 a^4}{D_2}\frac{\partial^2 \bar{w}_d}{\partial t^2}+\frac{1}{x}\frac{\partial}{\partial x}\left[xY_d^m\frac{\mathrm{d}\bar{w}_s}{\mathrm{d}x}+\frac{4}{x}Y_s^m\frac{\partial \bar{w}_d}{\partial x}+xY_d^m\frac{\partial \bar{w}_d}{\partial x}\right]-4\hat{T}\frac{1}{x}\frac{\partial}{\partial x}\left(x\frac{\partial \bar{w}_d}{\partial x}\right) \qquad 0<x<1$$

Boundary conditions at center $x = 0$:

$$\left.\frac{\partial \bar{w}_d}{\partial x}\right|_{x=0}=0\,, \tag{51a}$$

$$\left.Y_d^m\right|_{x=0}=\text{finite} \tag{51b}$$

Boundary conditions on circumference $x = 1$:

$$\left.\bar{w}_d\right|_{x=1}=0\,, \tag{52a}$$

$$\left[\nu\frac{\partial}{\partial x}(Y_d^m)+(1-\nu)Y_d^m\right]_{x=1}=0 \tag{52b}$$

$$\left[\frac{\partial^2 \bar{w}_d}{\partial x^2}+\nu\frac{\partial \bar{w}_d}{\partial x}\right]_{x=1}=0 \tag{52c}$$

5 STATIC SOLUTIONS

For the nonlinear static equations and boundary conditions of the boundary value problem derived above, static solutions of slopes $X_s(y)$ and forces $Y_s^m(y)$ can be represented in (exact) series expansion forms [14]:

$$X_s(y)=\sum_{i=1}^{\infty}A_i y^i \tag{53a}$$

$$Y_s^m(y)=\sum_{i=1}^{\infty}B_i y^i, \qquad 0\le y\le 1 \tag{53b}$$

where A_i and B_i are constant coefficients. Substituting the series solutions Eqs. (53) into static equations, Eqs. (45) and (46), and grouping coefficients of y_i one can obtain the recurrence equations for coefficients A_i and B_i:

$$A_i=\frac{1}{i(i-1)}\sum_{j=1}^{i-1}A_j B_{i-j}-\hat{T}A_{i-1} \tag{54a}$$

$$B_i=\frac{-1}{2i(i-1)}\sum_{j=1}^{i-1}A_j A_{i-j} \qquad i=2,3,4,... \tag{54b}$$

It is observed that only A_1 and B_1 are independent constants, and the others are dependent constants. As long as *A1* and *B1* are determined by the boundary conditions, other coefficients *Ai* and *Bi* can be calculated from the recurrence equations. Accordingly, static series solutions are completed. The series solutions of $Y_s^m(y)$ and $X_s(y)$ satisfy the boundary conditions at y=0, Eqs. (47). Substituting the assumed series solutions $Y_s^m(y)$ and $X_s(y)$ into the boundary conditions at y=1, Eqs. (48), yields

$$\sum_{i=1}^{\infty}\left[\left(1+\nu-2i\right)B_i\right]=0 \tag{55a}$$

$$\sum_{i=1}^{\infty}\left[\left(1-\nu-2i\right)A_i\right]=V \tag{55b}$$

A_i and B_i can be determined from the nonlinear algebraic equations Eqs. (55a, b) using the Newton-Raphson iteration method [15]. Define

$$\alpha\left(A_1,B_1\right)=\sum_{i=1}^{\infty}\left[\left(1-\nu-2i\right)A_i\right]-V\,,\qquad \beta\left(A_1,B_1\right)=\sum_{i=1}^{\infty}\left[\left(1+\nu-2i\right)B_i\right] \tag{56}$$

$$\bar{A}_1=A_1+\Delta_1\,,\qquad \bar{B}_1=B_1+\Delta_2 \tag{57}$$

in which

$$\Delta_1=\frac{1}{\Delta}\left[\beta\left(A_1,B_1\right)\frac{\partial}{\partial B_1}\alpha\left(A_1,B_1\right)-\alpha\left(A_1,B_1\right)\frac{\partial}{\partial B_1}\beta\left(A_1,B_1\right)\right] \tag{58a}$$

$$\Delta_2=\frac{1}{\Delta}\left[\alpha\left(A_1,B_1\right)\frac{\partial}{\partial A_1}\beta\left(A_1,B_1\right)-\beta\left(A_1,B_1\right)\frac{\partial}{\partial A_1}\alpha\left(A_1,B_1\right)\right] \tag{58b}$$

and

$$\Delta=\det\begin{bmatrix}\dfrac{\partial}{\partial A_1}\alpha\left(A_1,B_1\right) & \dfrac{\partial}{\partial B_1}\alpha\left(A_1,B_1\right)\\ \dfrac{\partial}{\partial A_1}\beta\left(A_1,B_1\right) & \dfrac{\partial}{\partial B_1}\beta\left(A_1,B_1\right)\end{bmatrix}\neq 0 \tag{58c}$$

$\bar{A}_1$ and $\bar{B}_1$ are, respectively, the iteration values of A_1 and B_1 ; Δ_1 and Δ_2 are the correction factors of A_1 and B_1 at each iteration. The partial derivatives $\partial\alpha/\partial A_1$, $\partial\alpha/\partial B_1$, $\partial\beta/\partial A_1$, and $\partial\beta/\partial B_1$ can be determined from the definitions of $\alpha\left(A_1,B_1\right)$ and $\beta\left(A_1,B_1\right)$. These iterations are repeated until they reach their prescribed limits, say $|\alpha|$, $|\beta|$, $|\Delta_1|$ and $|\Delta_2|$ are smaller than 10^{-4}. Accordingly, a set of A_1 and B_1 are determined for a set of given control voltages V and temperatures T^*. Using the recurrence equations, one can determine all other A_i's and B_i's, and further the nonlinear static solutions of slope $X_s(y)$ and static force $Y_s^m(y)$. Knowing the slope, one can determine the static deflections $\bar{w}_s$ and w_s of the nonlinear circular plate subjected to voltage and temperature excitations.

6 DYNAMIC SOLUTIONS

It is assumed that the FG circular plate is oscillating in the vicinity of the nonlinearly deformed static equilibrium position. FG index, voltage and temperature effects to the natural frequencies and amplitude/frequency relations are investigated in this section. Neglect the nonlinear terms in the normalized dynamic equations, and then assume following harmonic solutions of displacement and dynamic force

$$\bar{w}_d(x,t)=R_d(x)\sin(\omega_n t) \tag{59a}$$

$$Y_d^m(x,t)=S_d(x)\sin(\omega_n t) \tag{59b}$$

where ω_n is the natural frequency; $R_d(x)$ and $S_d(x)$ are the (linear) eigenfunctions or mode shape functions of $\bar{w}_d(x,t)$ and $Y_d^m(x,t)$, respectively. $R_d(x)$ defines the mode shape function, and $S_d(x)$ defines the spatial force

distribution. Both $R_d(x)$ and $S_d(x)$ have to satisfy the boundary conditions, and they are also assumed in the series expansion forms. Substituting Eqs. (59a, b) into the dynamic equations and boundary conditions, Eqs. (49)-(52), yields

$$x\frac{d}{dx}\left(\frac{1}{x}\frac{d}{dx}\left[x^2 S_d(x)\right]\right) = -2\frac{d\bar{w}_s}{dx}\frac{dR_d}{dx} \tag{60}$$

$$\frac{1}{x}\frac{d}{dx}\left\{x\frac{d}{dx}\left[\frac{1}{x}\frac{d}{dx}\left(x\frac{d}{dx}(R_d(x))\right)\right]\right\} = \lambda R_d(x) + \frac{1}{x}\frac{d}{dx}\left[2xS_d(x)\frac{d\bar{w}_s}{dx} + \frac{4}{x}Y_s^m\frac{dR_d}{dx}\right] - 4\hat{T}\frac{1}{x}\frac{d}{dx}\left[x\frac{dR_d}{dx}\right],\ 0 < x < 1 \tag{61}$$

where λ is the eigenvalue and $\lambda = I_1\frac{a^4}{D_2}\omega_n^2$. Boundary conditions become:

Center *x*=0:

$$\left.\frac{dR_d}{dx}\right|_{x=0} = 0 \tag{62a}$$

$$S_d(x)\big|_{x=0}: \text{finite} \tag{62b}$$

Circumference x=1:

$$R_d\big|_{x=1} = 0, \tag{63a}$$

$$\left[\nu\frac{d}{dx}\left[S_d(x)\right] + (1-\nu)S_d(x)\right]_{x=1} = 0 \tag{63b}$$

$$\left[\frac{d^2R_d}{dx^2} + \nu\frac{dR_d}{dx}\right]_{x=1} = 0 \tag{63c}$$

Again, assume the eigenfunctions take the series expansion forms:

$$R_d(x) = \sum_{i=0}^{\infty} a_i x^{2i} \tag{64a}$$

$$S_d(x) = \sum_{i=0}^{\infty} b_i x^{2i} \tag{64b}$$

where a_i and b_i are constants determined by eigenvalue equations and boundary conditions. The series solutions $R_d(x)$ and $S_d(x)$ satisfy the boundary conditions at $x = 0$. Assume a_i and b_i, be represented by the linear combinations of independent constants a_0, a_1 and b_0.

$$a_i = f_{i1}a_0 + f_{i2}a_1 + f_{i3}b_0 \tag{65a}$$

$$b_i = g_{i1}a_0 + g_{i2}a_1 + g_{i3}b_0,\quad i = 1,2,3,\ldots \tag{65b}$$

where f_{ij} and g_{ij} are to be determined. Substituting the series expressions of modes $R_d(x)$ and forces $S_d(x)$ into the dynamic equations, one can derive a set of recurrence equations of a_i and b_i. Then, using expressions of a_i and b_i of Eqs. (65a, b), one can further determine the coefficients f_{ij} and g_{ij}

$$f_{01} = 1,\quad f_{02} = f_{03} = 0 \tag{66}$$

$$f_{11} = 0,\quad f_{12} = 1,\quad f_{13} = 0 \tag{67}$$

$$g_{01}=0,\quad g_{02}=0,\quad g_{03}=1 \tag{68}$$

$$g_{ik}=-\frac{2}{i(i+1)}\sum_{j=1}^{i} jf_{jk}A_{i-j+1},\qquad i=1,2,3,\ldots,\quad k=1,2,3 \tag{69}$$

$$f_{21}=\lambda/64,\quad f_{22}=(B_1-T^*)/4,\quad f_{23}=A_1/8 \tag{70}$$

$$f_{31}=\left[A_1g_{11}+4f_{21}(B_1-T^*)\right]/36, \tag{71a}$$

$$f_{32}=\left\{\lambda+32B_2+16\left[A_1g_{12}+4f_{22}(B_1-T^*)\right]\right\}/24, \tag{71b}$$

$$f_{33}=\left[A_1g_{13}+4f_{23}(B_1-T^*)+A_2\right]/36, \tag{71c}$$

$$f_{(i+2)k}=\left[\lambda f_{ik}-16T^*(i+1)^2+8(i+1)\times\sum_{j=1}^{i+1}(2jf_{ik}B_{i-k+2}+A_jg_{(i-j+1)k})\right]\times\left[4(i+1)(i+2)\right]^{-2},\ i=2,3,4,\ldots,\ k=1,2,3. \tag{72}$$

Substituting these coefficients into the boundary conditions at x=1, one can obtain an explicit matrix representation of the eigenvalue equation.

$$\begin{bmatrix} h_{11} & h_{12} & h_{13} \\ h_{21} & h_{22} & h_{23} \\ h_{31} & h_{32} & h_{33} \end{bmatrix}\begin{bmatrix} a_0 \\ a_1 \\ b_0 \end{bmatrix}=\begin{bmatrix}0\end{bmatrix} \tag{73}$$

where h_{ij} are defined by

$$h_{1k}=\sum_{i=0i1}^{\infty} f_{ik},\qquad k=1,2,3 \tag{74a}$$

$$h_{2k}=\sum_{i=0}^{\infty}\left[i\nu+i(2i-1)\right]f_{ik},\qquad k=1,2,3. \tag{74b}$$

$$h_{3k}=\sum_{i=0}^{\infty}\left[2i\nu+(1-\nu)\right]g_{ik},\qquad k=1,2,3. \tag{74c}$$

These h_{ik} coefficients are functions of eigenvalues λ, and accordingly, the determinant of the coefficient matrix leads to a nonlinear characteristic equation. Using the Newton-Raphson iteration method [15], one can calculate eigenvalues and furthermore natural frequencies and mode shape functions of the nonlinear FG circular plate.

7 NUMERICAL ANALYSIS

To ensure the accuracy of the present analysis, an illustrative example is solved. The relevant material properties are listed in Table 1. Since there are no appropriate comparison results available for the problems being analyzed in this paper, we decided to verify the validity of obtained results by comparing to those of FEM results. Our FEM model for piezo-FG plate comprises: a 3D 8-noded solid element with 4 DOF per node (3 translation, temperature) in the host plate element and 6 DOF per node (3 translation, temperature, voltage and magnetic properties) in the piezoelectric element. Table 2 compares the present results of normalized dimensionless central deflections $W_s=\sqrt{3(1-\nu^2)}(w_s/h_f)$ with finite element solutions in analyzing the effect of normalized dimensionless piezoelectric voltages $V=\sqrt{3(1-\nu^2)}e_{31}(h_f+h_p)V^*/(2D_2h_f)$ to the normalized dimensionless center deflections at various normalized temperatures $(T^*=(a^2N^t/4D_2))$ in which a nonlinear deflection-voltage relationship can be observed. As it is seen from Table 2 the maximum estimated difference of the proposed solution with finite element method is about 0.079% and a close correlation between these results validates the proposed method of solution.

Table 1
Material properties [5]

Material	Property					
	E (GPa)	ρ (kg/m^3)	ν	α (1/°C)	κ (W/mK)	d_{31}, d_{32}(m/V)
Aluminum	70	2707	0.3	23e-6	204	-
Alumina	380	3800	0.3	7.4e-6	10.4	-
PZT	63	7600	0.3	1.2e-4	0.17	1.79e-10

Table 2
Normalized dimensionless center deflections versus normalized applied voltages for various normalized temperatures computed by two methods (present series solution and FEM) (v=0.3, n=1000)

	Normalized Temperature					
(V)	$T^*=0$			$T^*=0.2$		
	Present	FEM	Diff. (%)	Present	FEM	Diff. (%)
0	0	0	0	0	0	0
0.4	0.3537	0.3538	0.041	0.4788	0.4790	0.042
0.8	0.5982	0.5985	0.048	0.7550	0.7553	0.044
1.2	0.7681	0.7685	0.055	0.9310	0.9315	0.057
1.6	0.8925	0.8930	0.057	1.0596	1.0603	0.059
2	0.9924	0.9930	0.065	1.1640	1.1648	0.067
2.4	1.0777	1.0784	0.068	1.2517	1.2526	0.071
2.8	1.1509	1.1517	0.071	1.3254	1.3264	0.072
(V)	$T^*=0.5$			$T^*=0.8$		
	Present	FEM	Diff. (%)	Present	FEM	Diff. (%)
0	0	0	0	0	0	0
0.4	0.6633	0.6636	0.043	0.8659	0.8663	0.044
0.8	0.9569	0.9573	0.045	1.1347	1.1352	0.046
1.2	1.1380	1.1387	0.058	1.3118	1.3126	0.060
1.6	1.2746	1.2754	0.060	1.4601	1.4610	0.062
2.0	1.3776	1.3785	0.068	1.5581	1.5592	0.070
2.4	1.4643	1.4653	0.072	1.6458	1.6470	0.074
2.8	1.5510	1.5522	0.075	1.7653	1.7666	0.076

In general, a higher temperature induces higher deflections of the plate, and the deflection at each temperature is attenuated when the control voltage increase sand the effect of imposed voltage to the center deflection is nonlinear and this effect is predominant in fewer voltage amounts. This effect can also be seen in the case of considering the temperature environment effect. For example, when $T^*=0.2$ by increasing the imposed voltage from 0.6 to 1.2 (100%) the normalized dimensionless center deflections increases about 46.8% while it increases about 34.5% when the imposed voltage increases from 1.2 to 2.4 (100%) and in the case of $T^*=0.5$ by increasing the imposed voltage from 0.6 to 1.2 (100%) the normalized dimensionless center deflections increases about 36.5% while it increases about 28.7% when the imposed voltage increases from 1.2 to 2.4 (100%) . Having validated the foregoing formulations, we begin to study the large amplitude vibration behavior of FG laminated circular plate subjected to thermo-electro-mechanical loading. The results for laminated plates with isotropic substrate layers (that is, the substrate is purely metallic or purely ceramic) and with graded substrate layers (various n) are given in both tabular and graphical forms. To investigate the effect of the applied actuator voltage on the non-linear thermo-electromechanical vibration, nonlinear normalized center deflection of various graded plates (n=0.0.1, 0.5, 1, 10, 1000) under various applied normalized voltages (V=0, 0.2, 0.3, 0.5, and 1) are tabulated in Table 3. Also the Figs 1-4 shows the effects of the applied actuator voltage, FGM gradient index and normalized temperature on nonlinear normalized center deflection of piezoelectric coupled circular FGM plate in detail. It can be noted from the figures that by adjusting the actuator voltage, one can control the shape as well as the deflection of the FGM plate. Also it is

obvious that by increasing the FGM gradient index the normalized center deflection will increase in a nonlinear manner. For instance, Figs. 1 and 2 depict the normalized temperature and voltage effects to the center deflection of two graded plates (n=0.5 and 10). It shows that increasing the normalized temperature makes the center deflection increase in various voltages but this effect is predominant in higher voltages. Also in Fig. 3 and 4 we examine the effect of the temperature gradient on the non-linear thermo-electro-mechanical behavior (center deflection) of FGM plates under two imposed normalized voltages (V= 0, 0.2). As demonstrated by the figures, the temperature field with the larger gradient will lead to greater deflections. It is also obvious from these figures that, by increasing the material gradients, the normalized center deflection would be increased in various temperature fields and larger thermal gradients will lead to greater deflections. This trend can be seen in various material gradients. This means that the non-linear deflection can be controlled by applying the appropriate voltage in the piezoelectric actuator layers.

Table 3
FGM index and normalized voltage effects to the nonlinear center deflection

Normalized Temp. (T^*)	FGM index (n) / Normalized Voltage (V)									
	Metal					n=10				
	V=0	V=0.2	V=0.3	V=0.5	V=1	V=0	V=0.2	V=0.3	V=0.5	V=1
0.0	0.0000	0.1820	0.2724	0.3924	0.6925	0.0000	0.1206	0.1805	0.2601	0.4590
0.2	0.0060	0.2738	0.3869	0.5213	0.8573	0.0040	0.1815	0.2564	0.3455	0.5681
0.4	0.0162	0.3654	0.5010	0.6421	0.9949	0.0108	0.2422	0.3320	0.4255	0.6593
0.6	0.0332	0.4706	0.6169	0.7596	1.1164	0.0220	0.3119	0.4089	0.5034	0.7399
0.8	0.0516	0.6071	0.7400	0.8808	1.2329	0.0342	0.4024	0.4905	0.5838	0.8171
	n=1					n=0.5				
	V=0	V=0.2	V=0.3	V=0.5	V=1	V=0	V=0.2	V=0.3	V=0.5	V=1
0.0	0.0000	0.0992	0.1484	0.2138	0.3773	0.0000	0.0939	0.1405	0.2024	0.3572
0.2	0.0033	0.1492	0.2108	0.2840	0.4670	0.0031	0.1413	0.1996	0.2689	0.4422
0.4	0.0088	0.1991	0.2729	0.3498	0.5420	0.0084	0.1885	0.2584	0.3312	0.5132
0.6	0.0181	0.2564	0.3361	0.4138	0.6082	0.0171	0.2428	0.3183	0.3919	0.5759
0.8	0.0281	0.3308	0.4032	0.4799	0.6716	0.0266	0.3132	0.3818	0.4544	0.6360
	n=0.1					Ceramic (n=0)				
	V=0	V=0.2	V=0.3	V=0.5	V=1	V=0	V=0.2	V=0.3	V=0.5	V=1
0.0	0.0000	0.0838	0.1255	0.1807	0.3190	0.0000	0.0716	0.1072	0.1544	0.2725
0.2	0.0028	0.1261	0.1782	0.2401	0.3948	0.0024	0.1078	0.1522	0.2051	0.3373
0.4	0.0075	0.1683	0.2307	0.2957	0.4582	0.0064	0.1438	0.1971	0.2527	0.3915
0.6	0.0153	0.2168	0.2841	0.3499	0.5142	0.0131	0.1852	0.2428	0.2989	0.4393
0.8	0.0238	0.2796	0.3409	0.4057	0.5678	0.0203	0.2389	0.2912	0.3466	0.4851

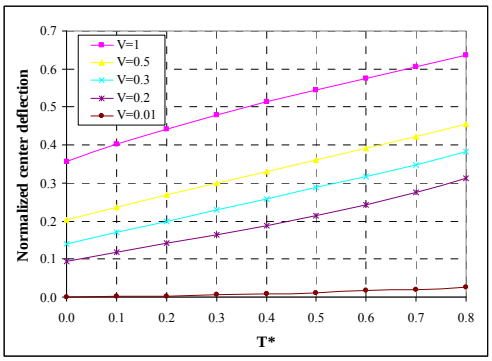

Fig. 1
Normalized Temperature effects to the center deflection for various values of Voltages (n=0.5).

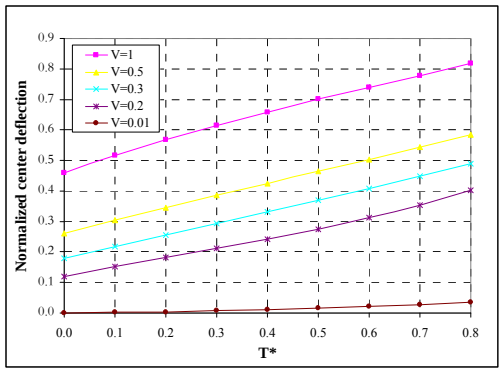

Fig. 2
Normalized Temperature effects to the center deflection for various values of Voltages (n=10).

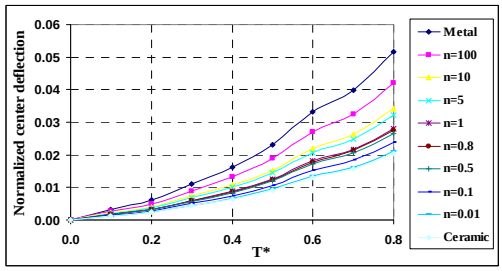

Fig. 3
Normalized temperature effects on nonlinear center deflection for various FGM indexes (V=0).

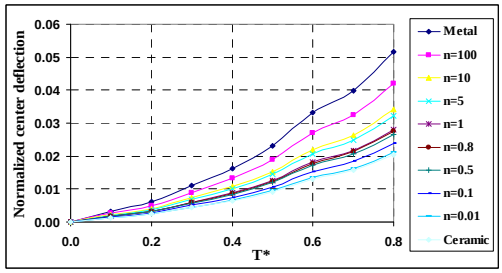

Fig. 4
Normalized temperature effects on nonlinear center deflection for various FGM indexes (V=0.2).

We examine in this section the effect of control voltages and thermal environment to the vibration characteristics of the piezoelectric laminated circular FG plate for various FGM indexes. To this end, Tables 4 and Figs. 5-8 show the nonlinear relationships between first natural frequencies $\omega_i a^2\sqrt{I_1/D_2}$ versus the normalized temperature in various normalized control voltages V. These free vibrations are assumed to be in the vicinity of the nonlinearly deformed static equilibrium position. Also, the effect of normalized temperature to the first natural frequency of the FG circular plate for various FGM indexes under various normalized control voltage are investigated and tabulated in Table 4 while the voltage dependent first natural frequency changes are plotted in Figs. 5-8 for various temperatures. It is seen that, imposed voltage has a significant effect on the first natural frequency of the structure and by increasing imposed voltage, the first natural frequency increases in a nonlinear manner. For instance, for FGM plate with n=10 by increasing the imposed voltage from 0 to 0.2 first natural frequency increases about 4.84% while by increasing the voltage from 0.2 to 0.3 first natural frequency increases about 15.12%. It is seen that, imposed thermal environment has a significant effect on the first natural frequency of the structure and by increasing imposed temperature, the first natural frequency decreases in a nonlinear manner. However, this thermal tendency of decreasing the natural frequency can be compensated and corrected with the control voltages V, as shown in Figs. 5-7.

Table 4
FGM index and normalized temperature effects to the first natural frequency for various normalized voltages

Normalized Voltage (V)	FGM index (n) / Normalized Temp. (T^*)							
	Metal				n=10			
	Normalized Temperature (T^*)				Normalized Temperature (T^*)			
	0	0.2	0.5	0.8	0	0.2	0.5	0.8
0.0	4.8891	4.4249	3.5293	2.3669	5.5359	5.0103	3.9962	2.6800
0.4	5.5796	5.67452	5.92735	6.49712	6.3178	6.4253	6.7116	7.3567
0.8	6.7141	7.26308	8.00595	8.71889	7.6024	8.2240	9.0652	9.8724
1.2	7.7799	8.452	9.37002	10.1564	8.8092	9.5702	10.6097	11.5001
1.6	8.6394	9.33903	10.3511	11.2809	9.7824	10.5746	11.7206	12.7734
2.0	9.3329	10.1399	11.2449	12.2285	10.5677	11.4814	12.7326	13.8464
2.4	9.9414	10.8734	12.0351	13.0241	11.2567	12.3120	13.6274	14.7472
2.8	10.5104	11.4499	12.6036	13.7116	11.9010	12.9647	14.2711	15.5257
3.0	10.7796	11.7344	12.9013	14.0447	12.2058	13.2869	14.6082	15.9028

Normalized Voltage (V)	FGM index (n) / Normalized Temp. (T^*)							
	n=1				n=0.5			
	Normalized Temperature				Normalized Temperature			
	0	0.2	0.5	0.8	0	0.2	0.5	0.8
0.0	7.4121	6.7083	5.3506	3.5883	8.2786	7.4926	5.9761	4.0078
0.4	8.4589	8.6028	8.9861	9.8499	9.4478	9.6085	10.0366	11.0014
0.8	10.1789	11.0111	12.1374	13.2182	11.3689	12.2984	13.5563	14.7635
1.2	11.7947	12.8136	14.2054	15.3975	13.1735	14.3116	15.8660	17.1976
1.6	13.0977	14.1584	15.6927	17.1023	14.6289	15.8136	17.5273	19.1017
2.0	14.1491	15.3725	17.0478	18.5389	15.8032	17.1696	19.0407	20.7062
2.4	15.0716	16.4845	18.2458	19.7451	16.8335	18.4117	20.3788	22.0534
2.8	15.9342	17.3585	19.1076	20.7874	17.7970	19.3878	21.3413	23.2176
3.0	16.3423	17.7899	19.5589	21.2924	18.2528	19.8696	21.8455	23.7815

Normalized Voltage (V)	FGM index (n) / Normalized Temp. (T^*)							
	n=0.1				Ceramic			
	Normalized Temperature				Normalized Temperature			
	0	0.2	0.5	0.8	0	0.2	0.5	0.8
0.0	10.1803	9.2138	7.3489	4.9285	11.2882	10.2165	8.1487	5.4648
0.4	11.6181	11.8158	12.3422	13.5287	12.8825	13.1017	13.6854	15.0009
0.8	13.9805	15.1236	16.6704	18.1549	15.5020	16.7694	18.4846	20.1307
1.2	16.1997	17.5992	19.5108	21.1482	17.9627	19.5145	21.6340	23.4497
1.6	17.9894	19.4462	21.5536	23.4897	19.9472	21.5625	23.8992	26.0460
2.0	19.4335	21.1138	23.4147	25.4628	21.5483	23.4116	25.9629	28.2339
2.4	20.7005	22.6412	25.0602	27.1195	22.9533	25.1051	27.7874	30.0708
2.8	21.8853	23.8416	26.2438	28.5511	24.2670	26.4362	29.0999	31.6582
3.0	22.4459	24.4340	26.8638	29.2446	24.8886	27.0931	29.7873	32.4272

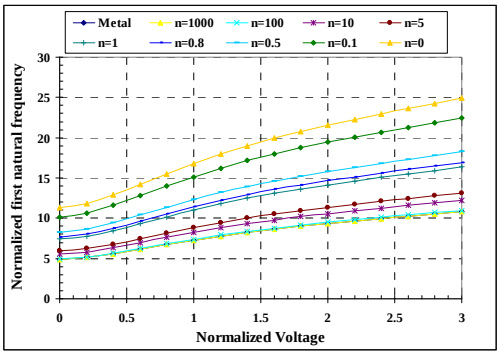

Fig. 5
Effect of normalized voltage to first natural frequency for various FGM indexes (T^*=0)

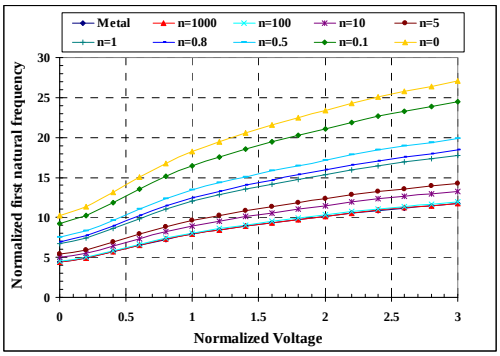

Fig. 6
Effect of normalized voltage to first natural frequency for various FGM indexes (T^*=0.2).

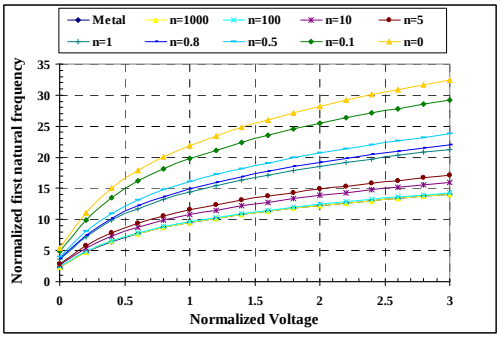

Fig. 7
Effect of normalized voltage to first natural frequency for various FGM indexes (T^*=0.8).

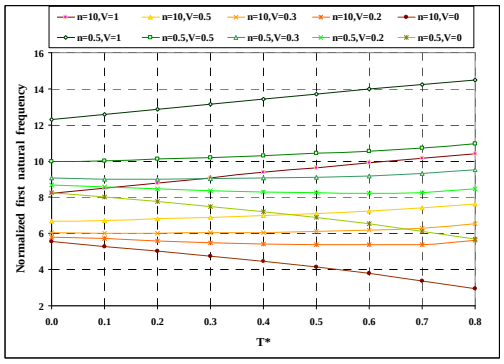

Fig. 8
Temperature effects on normalized first natural frequency for various normalized voltages (n=10 and n=0.5).

8 CONCLUSIONS

A circular FG plate coupled with piezoelectric layers subjected to temperature changes and control voltages are investigated based on classical plate theory. Voltage controlled natural frequencies of the first mode at various temperatures is studied. It is observed that a higher temperature induces higher deflections of the plate, and the deflection at each temperature is attenuated when the control voltage increases but this effect is predominant in higher voltages. Also by increasing the FGM gradient index, the normalized center deflection will increase in a nonlinear manner in various temperature fields. It is seen that, imposed thermal environment has a significant effect on the natural frequency of the structure and by increasing imposed temperature, the natural frequency decreases in a nonlinear manner for various FGM indexes and this effect is predominant in higher temperatures. Both the nonlinear static deflections and natural frequencies are influenced by the temperatures and control voltages and the static control voltages can be used to compensate nonlinear deflections.

9 APPENDIX A

$$
\begin{aligned}
&T_1 = T_2 + (T_U - T_L) - \frac{\kappa_c d + \kappa_m}{\kappa_m}(T_2 - T_L)\\
&T_2 = T_L + \left[\frac{\kappa_m}{ch_f}(T_U - T_L)\right] \Bigg/ \left[\frac{\kappa_p}{h_p} + \frac{\kappa_c d + \kappa_m}{ch_f}\right]\\
&A_0 = T_2\,, \quad A_1 = \frac{T_1 - T_2}{c}\,, \qquad A_2 = -\frac{T_1 - T_2}{c}\frac{\kappa_{cm}}{(N+1)\kappa_m}\\
&A_3 = \frac{T_1 - T_2}{c}\frac{\kappa_{cm}^2}{(2N+1)\kappa_m^2}\,, \qquad A_4 = -\frac{T_1 - T_2}{c}\frac{\kappa_{cm}^3}{(3N+1)\kappa_m^3}\\
&A_5 = \frac{T_1 - T_2}{c}\frac{\kappa_{cm}^4}{(4N+1)\kappa_m^4}\,, \qquad A_6 = -\frac{T_1 - T_2}{c}\frac{\kappa_{cm}^5}{(5N+1)\kappa_m^5}
\end{aligned}
\tag{A.1}
$$

where

$$
\begin{aligned}
&\kappa_{cm} = \kappa_c - \kappa_m\\
&c = 1 - \frac{1}{N+1}\frac{\kappa_{cm}}{\kappa_m} + \frac{1}{2N+1}\left(\frac{\kappa_{cm}}{\kappa_m}\right)^2 - \frac{1}{3N+1}\left(\frac{\kappa_{cm}}{\kappa_m}\right)^3 + \frac{1}{4N+1}\left(\frac{\kappa_{cm}}{\kappa_m}\right)^4 - \frac{1}{5N+1}\left(\frac{\kappa_{cm}}{\kappa_m}\right)^5\\
&d = 1 - \frac{\kappa_{cm}}{\kappa_m} + \left(\frac{\kappa_{cm}}{\kappa_m}\right)^2 - \left(\frac{\kappa_{cm}}{\kappa_m}\right)^3 + \left(\frac{\kappa_{cm}}{\kappa_m}\right)^4 - \left(\frac{\kappa_{cm}}{\kappa_m}\right)^5
\end{aligned}
\tag{A.2}
$$

REFERENCES

[1] Dong S., Du X., Bouchilloux P., Uchino K., 2002, Piezoelectric ring-morph actuation for valve application, *Journal of Electroceramics* **8**: 155-61.

[2] Cao L., Mantell S., Polla D., 2001, Design and simulation of an implantable medical drug delivery system using microelectromechanical systems technology, *Sensors Actuators A* **94**: 117-125.

[3] Reddy J.N., Cheng Z.Q., 2001, Three-dimensional solutions of smart functionally graded plates, *ASME Journal of Applied Mechanics* **68**: 234-241.

[4] Wang B.L., Noda N., 2001, Design of smart functionally graded thermo-piezoelectric composite structure, *Smart Materials and Structures* **10**: 189-193.

[5] Huang X.L., Shen H.S., 2006, Vibration and dynamic response of functionally graded plates with piezoelectric actuators in thermal environments, *Journal of Sound and Vibration* **289**: 25-53.

[6] Ebrahimi F., Rastgoo A., Kargarnovin M.H., 2008, Analytical investigation on axisymmetric free vibrations of moderately thick circular functionally graded plate integrated with piezoelectric layers, *Journal of Mechanical Science and Technology* **22**(16): 1056-1072.

[7] Ebrahimi F., Rastgoo A., 2008, Free vibration analysis of smart annular FGM plates integrated with piezoelectric layers, *Smart Materials and Structures* **17**(1): doi:10.1088/0964-1726/17/1/015044.

[8] Ebrahimi F., Rastgoo A., 2009, Nonlinear vibration of smart circular functionally graded plates coupled with piezoelectric layers, *International Journal of Mechanics and Materials in Design* **5**: 157-165.

[9] Reddy J.N., Praveen G.N., 1998, Nonlinear transient thermoelastic analysis of functionally graded ceramic-metal plate, *International Journal of Solids and Structures* **35**: 4457-4476.

[10] Brush D.O., Almroth B.O., 1975, *Buckling of Bars Plates and Shells*, McGraw-Hill, New York.

[11] Reddy J.N., 1999, *Theory and Analysis of Elastic Plates,* Taylor and Francis, Philadelphia.

[12] Efraim E., Eisenberger M., 2007, Exact vibration analysis of variable thickness thick annular isotropic and FGM plate, *Journal of Sound and Vibration* **299**: 720-738.

[13] Tzou H.S., 1993, *Piezoelectric Shells-Distributed Sensing and Control of Continua,* Kluwer, Dordrecht.

[14] Zheng X.J., Zhou Y.H., 1990, Analytical formulas of solutions of geometrically nonlinear equations of axisymmetric plates and shallow shells, *Acta Mechanica Sinica* **6**(1): 69-81.

[15] William H.P., Brain P.F., Sau A.T., 1986, *Numerical Recipes-the Art of Scientific Computing*, Cambridge University Press, New York.